Extropy Analysis of the Inactivity Times of the Failed Components in Coherent Systems with Applications to Estimation and Image Processing

Zohreh Pakdaman[1]* and Reza Alizadeh Noughabi[1,*]

[1] *Department of Statistics, University of Hormozgan, Hormozgan, Iran*

December 6, 2025

Abstract

This study presents a comprehensive examination of the extropy associated with the inactivity times of failed components in coherent systems. In contrast to conventional reliability measures that emphasize system inactivity or residual lifetime analysis, the proposed framework captures the underlying informational characteristics embedded in the inactivity times of failed components while the overall system remains operational. By employing system signatures, we derive closed-form representations for the extropy of these inactivity times and establish a series of stochastic bounds and comparative results that elucidate the influence of system structure and configuration. Furthermore, we assess the sensitivity of extropy through numerical experiments based on Weibull-distributed lifetimes. On the applied side, we develop two non-parametric estimators for the extropy of inactivity times of failed components in coherent systems. The proposed estimators' efficiency are demonstrated via simulated datasets and further illustrated through an image processing application, highlighting the practical relevance of the extropy-based approach in reliability and information-theoretic analysis.

Keywords and Phrases: Extropy, Non-parametric estimators, Order statistics, Stochastic order, System signature, Inactivity times of the failed components, Image processing.

AMS 2000 Subject Classification: Primary 62N05; Secondary 62F10.

1 Introduction

In reliability theory, one of the most intricate challenges arises when examining the behavior of components that have already failed but do not immediately lead to the breakdown of the overall system. Classical reliability analyses tend to focus on system lifetime distributions or the survival

*Corresponding authors.

E-mail: *zpakdaman@hormozgan.ac.ir* (Z. Pakdaman), *reza.alizadehn@hormozgan.ac.ir* (R. Alizadeh Noughabi).

probabilities of still-functioning components, often neglecting the hidden impact of those elements that have failed yet remain embedded within an operational structure. By emphasizing the concept of inactivity time, the duration during which a component remains failed while the system continues to perform, we gain valuable insights into the system's intrinsic resilience, interdependence among components, and long-term susceptibility to deterioration. The practical significance of this viewpoint can be illustrated through several distinct scenarios:

1- In a patient monitoring setup consisting of multiple sensors, such as heart rate, temperature, and oxygen level sensors, the system can continue to function even when one or more sensors have stopped working. These failed sensors accumulate an inactivity time while the system keeps monitoring through the remaining active units. Analyzing such durations helps biomedical engineers identify early degradation patterns, predict component lifespans, and design optimal replacement or calibration schedules before the system's overall reliability is compromised.

2- In large-scale distributed software systems, such as cloud platforms with numerous interdependent service modules, some components (e.g., authentication servers or data caches) may crash without immediately disrupting the entire service. These failed modules remain inactive within the architecture while other modules continue handling requests. Investigating the inactivity times of such modules enables software engineers to assess subsystem stability, determine optimal reboot or patch intervals, and enhance fault-tolerant designs for sustained reliability under load.

3- In urban traffic control systems composed of multiple sensors and controllers at intersections, the network remains operational even if certain sensors fail temporarily. These inactive sensors accumulate inactivity periods before the network's performance begins to degrade noticeably. Studying their inactivity times helps city engineers detect critical nodes, implement preventive maintenance, and strengthen the system's robustness against progressive failures.

Together, these examples demonstrate that the concept of inactivity time represents a crucial and complementary reliability measure. It quantifies how long failed components persist within an otherwise functional system, providing both theoretical understanding and practical guidance for enhancing structural robustness, improving maintenance strategies, and preventing cascading failures across complex engineered systems.

For a coherent system consisting of n components with overall lifetime denoted by $T(n)$, let the individual component lifetimes Y_i $(i = 1, \ldots, n)$ be independent and identically distributed (IID) random variables characterized by a common cumulative distribution function (CDF) $G(\cdot)$. The reliability structure of the system can be completely specified by its signature vector, an n-dimensional probability vector expressed as $\boldsymbol{s} = (s_1, s_2, \ldots, s_n)$, where each element $s_i = P(T(n) = Y_{i:n})$ represents the probability that system failure occurs precisely at the time of the ith order statistic $Y_{i:n}$, corresponding to the ith weakest component. By definition, the components of the signature satisfy the normalization constraint $\sum_{i=1}^{n} s_i = 1$. Hence, the signature provides a probabilistic characterization of how the overall system failure is influenced by the order in which individual component failures occur. A comprehensive exposition of the system signature framework can be found in Samaniego (2007).

Let the random variable $T(n)$ possess the probability density function (PDF) $g_{T(n)}(\cdot)$ and CDF $G_{T(n)}(\cdot)$. In this study, we focus on a particular class of coherent systems whose signature vectors take a degenerate form given by $\boldsymbol{s} = (0, \ldots, 0, s_i, s_{i+1}, \ldots, s_n), \quad i = 2, \ldots, n$, which corresponds to systems in which failures of the first $(i-1)$ components cannot directly cause system breakdown. Throughout the analysis, we assume that the system operation commences at time $t = 0$.

For simplicity in notation, we define $t - Y_{j:n}|Y_{j:n} < t < T$, $t - Y_{j:n}|Y_{j:n} < t < Y_{k:n}$, and $t - Y_{j:n}|Y_{l:n} < t < Y_{l+1:n}$ for $1 \leq j \leq l < k \leq n$ as $IT_{j,n}(t)$, $IY_{j,k,n}(t)$, and $IY^t_{l-j+1:l}$, respectively, throughout the rest of the paper. Additionally, assume that the CDF of $IT_{j,n}(t)$ (or $IY_{j,k,n}(t)$ or $IY^t_{l-j+1:l}$) is $G_{IT_{j,n}(t)}(.)$ (or $G_{IY_{j,k,n}(t)}(.)$ or $G_{IY^t_{l-j+1:l}}(.)$), respectively. From Goliforushani et al. (2012), we have

$$\bar{G}_{IT_{j,n}(t)}(y) = \sum_{k=i}^{n} q_k(t) \bar{G}_{IY_{j,k,n}(t)}(y), \tag{1}$$

where

$$\bar{G}_{IY_{j,k,n}(t)}(y) = \sum_{l=j}^{k-1} B_{l,j,k,n}(t)\, \bar{G}_{IY^t_{l-j+1:l}}(y), \tag{2}$$

$$\begin{aligned} \bar{G}_{IY^t_{l-j+1:l}}(y) &= \sum_{m=j}^{l} \binom{l}{m} \left(\frac{G(t-y)}{G(t)}\right)^m \left(1 - \frac{G(t-y)}{G(t)}\right)^{l-m} \\ &= \int_0^{\frac{G(t-y)}{G(t)}} j \binom{l}{j} u^{j-1}(1-u)^{l-j}\, du, \;\; 0 < y < t, \end{aligned} \tag{3}$$

$$q_k(t) = \frac{s_k \sum\limits_{l=j}^{k-1} \binom{n}{l} (\frac{G(t)}{\bar{G}(t)})^l}{\sum\limits_{m=i}^{n} \sum\limits_{l=j}^{m-1} s_m \binom{n}{l} (\frac{G(t)}{\bar{G}(t)})^l}, \tag{4}$$

and

$$B_{l,j,k,n}(t) = \frac{\binom{n}{l} (\frac{G(t)}{\bar{G}(t)})^l}{\sum\limits_{l=j}^{k-1} \binom{n}{l} (\frac{G(t)}{\bar{G}(t)})^l}. \tag{5}$$

Additionally, assume that the PDF of $IT_{j,n}(t)$ (or $IY_{j,k,n}(t)$ or $IY^t_{l-j+1:l}$) is $g_{IT_{j,n}(t)}(.)$ (or $g_{IY_{j,k,n}(t)}(.)$ or $g_{IY^t_{l-j+1:l}}(.)$), respectively. Therefore, we have

$$g_{IT_{j,n}(t)}(y) = \sum_{k=i}^{n} q_k(t) g_{IY_{j,k,n}(t)}(y), \tag{6}$$

where

$$g_{IY_{j,k,n}(t)}(y) = \sum_{l=j}^{k-1} B_{l,j,k,n}(t) g_{IY^t_{l-j+1:l}}(y), \tag{7}$$

and

$$g_{IY^t_{l-j+1:l}}(y) = j\binom{l}{j}\frac{g(t-y)}{G(t)}(\frac{G(t-y)}{G(t)})^{j-1}(1-\frac{G(t-y)}{G(t)})^{l-j},\ 0<y<t. \tag{8}$$

For coherent systems characterized by a signature vector of the form $\boldsymbol{s} = (0, \ldots, 0, s_i, s_{i+1}, \ldots, s_n)$ for $i = 2, \ldots, n$, the components that have already failed prior to a given time t continue to exert an implicit effect on the overall system performance, even though their individual failure times are not directly observable. In such cases, the system can be perceived as a "black box" since, while the system remains operational, the precise lifetimes of the failed components are hidden from observation. To characterize this hidden reliability behavior, we define the conditional probability function $\bar{G}_{IT_{j,n}(t)}(y) = P(t - Y_{j:n} > y \mid Y_{j:n} < t < T)$, which represents the survival function associated with the inactivity times of the failed components. This function quantifies the probability that the inactivity duration of the jth component, which failed before time t, exceeds a specified value y given that the system as a whole is still functioning at time t. The condition $Y_{j:n} < t$ indicates that the jth component has already failed before t, whereas $t < T$ ensures that the system lifetime has not yet expired. Consequently, the conditional probability $\bar{G}_{IT_{j,n}(t)}(y)$ captures the stochastic behavior of component inactivity within an operating system, serving as a fundamental measure of how long failed components remain dormant without immediately compromising overall system reliability.

A substantial body of research has addressed the study of inactivity times in coherent systems under a variety of modeling assumptions and reliability structures. Notable contributions include the works of Khaledi and Shaked (2007), Li and Zhao (2008), Zhang (2010), Zhang and Yang (2010), Goliforushani and Asadi (2011), Goliforushani et al. (2012), Tavangar (2015), Navarro et al. (2017), Navarro and Calì (2019), Guo et al. (2022), Rao and Naqvi (2024), and Zhang (2025). These studies collectively provide a broad theoretical and methodological foundation for analyzing the stochastic behavior of component inactivity and its implications for system reliability assessment.

Classical reliability indices, including mean inactivity time and conventional hazard-type measures, often fail to adequately represent the inherent complexity that emerges when certain components of a coherent system have already failed, yet the system as a whole remains operational. Such traditional summaries typically overlook the subtle distributional features and latent dependencies that characterize the inactivity times of failed components still embedded within a functioning structure. To address this shortcoming, we adopt an information-theoretic framework and introduce the notion of extropy as a fundamental measure for assessing the structural complexity associated with inactivity times. Within the broader context of information theory, one of the foundational constructs for quantifying uncertainty in random phenomena is entropy. Introduced by Shannon (1948), entropy provides a principled means of measuring the expected uncertainty in a probabilistic model. For a continuous random variable X with probability density function (PDF) $f(x)$, the Shannon entropy is defined as $H(X) = -E[\log f(X)]$, where log denotes the natural logarithm. In contrast, extropy is proposed as the dual concept to entropy. While entropy traditionally reflects disorder and unpredictability, extropy has been interpreted in subsequent literature as a measure of structural coherence, vitality, and the inherent tendency of systems toward organization, stability, and potential growth. Formally, Lad et al. (2015) defined the extropy of a random variable X with PDF $f(x)$ as

$$J(X) = -\frac{1}{2}\int_{-\infty}^{+\infty} f^2(x)\,dx = -\frac{1}{2}\int_0^1 f(F^{-1}(u))\,du, \tag{9}$$

where $F^{-1}(\cdot)$ denotes the inverse of the CDF of X.

A growing body of literature has explored extropy and its applications in analyzing the informational properties of reliability models. For a detailed account of the theoretical and applied aspects of extropy within reliability and information theory, the reader is referred to the works of Qiu (2017), Qiu and Jia (2018a, 2018b), Kayal (2019), Jose and Sathar (2019), Jahanshahi et al. (2020), Pakdaman and Hashempour (2021), Chakraborty and Pradhan (2022, 2023a, 2023b, 2024), and Pakdaman and Noughabi (2025a, 2025b, 2025c).

This study focuses on the analysis of extropy associated with the inactivity times of failed components within a coherent system that remains operational at time t, as formalized in Equation (1). The structure of the paper is as follows: Section 2 provides a comprehensive formulation of the extropy for inactivity durations of failed components in still-functioning systems, employing the conditional coefficients vector and deriving relevant stochastic comparisons and theoretical bounds. Section 3 introduces a new divergence measure aimed at capturing the structural complexity inherent in the inactivity times of failed elements embedded in active systems. In Section 4, we propose two non-parametric estimators for estimating the extropy of inactivity times of failed components within a coherent system and demonstrate their application using simulated data. Also, in Section 5, the efficiency and performance of these estimators are demonstrated through an image processing application. Finally, Section 6 concludes with a synthesis of the main theoretical contributions and practical implications, emphasizing the role of inactivity times of failed components in shaping the long-term reliability of coherent systems.

2 Extropy of inactivity times of the failed components

Let $Y_1, Y_2, \ldots, Y_n$ denote the IID lifetimes of n components, each following the CDF $G(\cdot)$. Consider a coherent system of order n characterized by the signature vector $\boldsymbol{s} = (0, \ldots, 0, s_i, s_{i+1}, \ldots, s_n)$

for $i = 2, \ldots, n$. Let $T(n)$ represent the system lifetime, with the PDF $g_{T(n)}(\cdot)$ and CDF $G_{T(n)}(\cdot)$. The primary objective is to evaluate the extropy associated with the inactivity times of failed components, that is, to compute the extropy of the conditional random variable $t - Y_{j:n} \mid Y_{j:n} < t < T$. This quantity reflects the informational structure of component inactivity within an operational system, capturing how uncertainty is distributed across the durations for which failed components remain inactive while the system continues to function.

In this section, we derive an analytical expression for the extropy of the inactivity times of failed components in a coherent system whose reliability configuration is specified by the signature vector $\boldsymbol{s} = (0, \ldots, 0, s_i, s_{i+1}, \ldots, s_n)$ for $i = 2, \ldots, n$. By employing Equations (6) and (9), the extropy of $IT_{j,n}(t)$ can be formulated as

$$\begin{aligned}
J\left(IT_{j,n}(t)\right) &= -\frac{1}{2}\int_0^t g^2_{IT_{j,n}(t)}(y)\ dy \\
&= -\frac{1}{2}\int_0^t \Big(\sum_{k=i}^{n} q_k(t) g_{IY_{j,k,n}(t)}(y)\Big)^2\ dy \\
&= -\frac{1}{2}\int_0^t \Big(\sum_{k=i}^{n}\sum_{l=j}^{k-1} q_k(t) B_{l,j,k,n}(t) g_{IY^t_{l-j+1:l}}(y)\Big)^2\ dy \\
&= -\frac{1}{2}\int_0^t \Big(\sum_{k=i}^{n}\sum_{l=j}^{k-1} q_k(t) B_{l,j,k,n}(t) j\binom{l}{j}\frac{g(t-y)}{G(t)}\big(\frac{G(t-y)}{G(t)}\big)^{j-1}\big(1-\frac{G(t-y)}{G(t)}\big)^{l-j}\Big)^2\ dy \\
&= -\frac{1}{2}\int_0^1 \Big(\sum_{k=i}^{n}\sum_{l=j}^{k-1} q_k(t) B_{l,j,k,n}(t) j\binom{l}{j}(1-u)^{j-1}u^{l-j}\Big)^2\ du. \qquad (10)
\end{aligned}$$

In this context, $IY^t_{l-j+1:l}$ represents the $(l-j+1)$-th order statistic among l independent and identically distributed random variables having the same distribution as $(t - X \mid X < t)$, whose corresponding CDF is given by $\frac{G(t-x)}{G(t)}$. In the subsequent development, our aim is to reexpress the extropy corresponding to the inactivity times of failed components in a form that is analytically more tractable. To achieve this, we begin by simplifying specific constituent terms in Equation (10), which facilitates a more compact and interpretable formulation of the overall expression. As an initial step in this refinement process, we focus on the multiplicative interaction between $q_k(t)$ and $B_{l,j,k,n}(t)$, for which a reduced form is obtained as follows:

$$q_k(t) B_{l,j,k,n}(t) = \frac{s_k\binom{n}{l}\big(\frac{G(t)}{\bar{G}(t)}\big)^l}{\sum\limits_{m=i}^{n} s_m\binom{n}{l}\big(\frac{G(t)}{\bar{G}(t)}\big)^l}. \qquad (11)$$

By substitution of Equation (11) into Equation (10), we immediately arrive at the following simplified representation:

$$J\left(IT_{j,n}(t)\right) = -\frac{1}{2}\int_0^t \Big(\frac{\bar{G}^n(t)}{\sum\limits_{m=i}^{n} s_m\big(G_{Y_{j:n}}(t)-G_{Y_{m:n}}(t)\big)}\sum_{k=i}^{n} s_k \sum_{l=j}^{k-1} j\binom{l}{j}\binom{n}{l}\Big(\frac{G(t)}{\bar{G}(t)}\Big)^l \times (1-u)^{j-1}u^{l-j}\, du\Big)^2\, du. \tag{12}$$

Equation (12) establishes a systematic framework for computing the extropy of the inactivity times of failed components in a coherent system that continues to operate at time t. In this framework, the relative contributions of inactive components are quantified through the conditional coefficient vector $\mathbf{q}(t) = (0, 0, \ldots, 0, q_i(t), \ldots, q_n(t))$, which serves as the system's conditional signature. Each entry $q_k(t)$ represents the probability that the kth failed component, with lifetime $Y_{k:n}$, influences the inactivity structure, conditional on the system remaining functional while components $Y_{k:n}$ for $k = 1, \ldots, i$ have already failed. This approach provides reliability engineers with a nuanced understanding of the interdependence between failed and surviving components, emphasizing how the inactivity of lower-order elements interacts with the continuing operation of higher-order components. Consequently, the conditional signature vector $\mathbf{q}(t)$ offers a valuable analytical tool for evaluating latent system vulnerabilities and for designing systems where distinguishing between failed component inactivity and overall system survival is essential. The following example demonstrates the practical computation of extropy based on Equation (12).

Example 1 *Consider a coherent system characterized by the signature vector* $\boldsymbol{s} = (0, \frac{1}{6}, \frac{12}{7}, \frac{1}{4})$, *which consists of four statistically IID components. Each component lifetime follows a Weibull distribution with shape parameter* $\alpha > 0$ *and scale parameter* $\lambda > 0$. *Its PDF is defined as* $g(y) = \frac{\alpha}{\lambda}\left(\frac{y}{\lambda}\right)^{\alpha-1}\exp\left[-\left(\frac{y}{\lambda}\right)^{\alpha}\right],\ y > 0$. *As is well known, the reversed hazard rate function of the Weibull distribution is monotonically decreasing when the shape parameter satisfies* $\alpha \le 1$. *For* $\alpha > 1$, *the reversed hazard rate function exhibits a unimodal behavior, increasing initially and then decreasing after attaining a unique maximum value. According to the structure induced by the signature, the system lifetime is given by* $T(4) = \max(Y_1, \min(Y_2, Y_3), \min(Y_3, Y_4))$. *In what follows, by applying Equation* (12), *we proceed to derive the extropy associated with the inactivity times of failed components of this system. For the present illustration, we fix the auxiliary parameters as* $n = 4$, $i = 2$, $j = 2$, *and* $\lambda = 1.5$. *Under these settings, the functional form* $J(IT_{2,4}(t))$ *can be derived analytically for the Weibull model. Specifically, for the two distinct shape parameters* $\alpha = 0.5$ *and* $\alpha = 2$, *one obtains the following explicit closed-form representations as*

$$J(IT_{2,4}(t)) = -\frac{181500 + 23100\big(e^{(\frac{t}{1.5})^{0.5}} - 1\big) + 1176\big(e^{(\frac{t}{1.5})^{0.5}} - 1\big)^2}{10\Big(165 + 14\big(e^{(\frac{t}{1.5})^{0.5}} - 1\big)\Big)^2}, \tag{13}$$

and

$$J(IT_{2,4}(t)) = -\frac{181500 + 23100\big(e^{(\frac{t}{1.5})^2} - 1\big) + 1176\big(e^{(\frac{t}{1.5})^2} - 1\big)^2}{10\Big(165 + 14\big(e^{(\frac{t}{1.5})^2} - 1\big)\Big)^2}, \tag{14}$$

respectively.

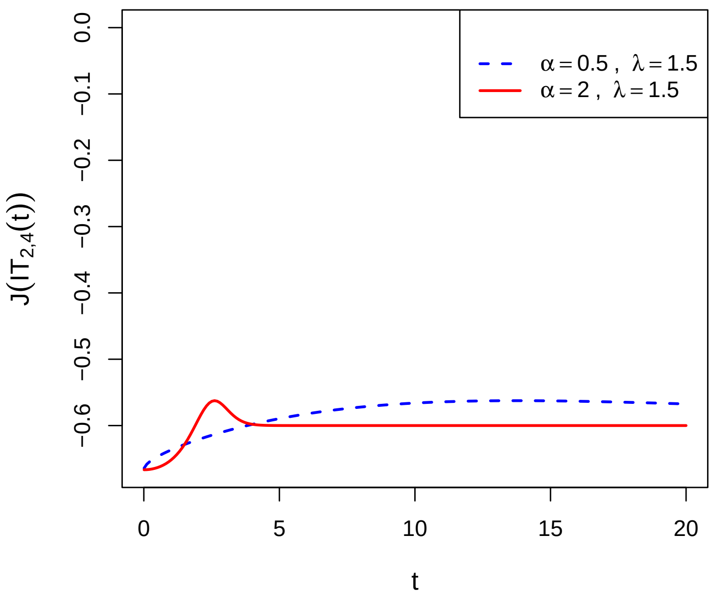

Figure 1: Extropy values $J\left(IT_{2,4}(t)\right)$ of inactivity times of failed components of system with lifetime $T(4) = \max(Y_1, \min(Y_2, Y_3), \min(Y_3, Y_4))$ in Example 1.

The plotted curve in Figure 1 represents the extropy of inactivity times of failed components in the coherent system $T(4) = \max(Y_1, \min(Y_2, Y_3), \min(Y_3, Y_4))$ for the Weibull distribution with $\lambda = 1.5$ and two shape parameters $\alpha = 0.5$ and $\alpha = 2$. For $\alpha = 0.5$, the extropy of inactivity times of failed components increases gradually as time t increases, indicating that the uncertainty associated with the inactive periods of the system components grows progressively. This behavior reflects the high variability of component lifetimes: when components follow a heavy-tailed distribution, longer inactivity periods are more unpredictable, leading to a gradual increase in extropy. For$\alpha = 2$, the extropy initially increases as time t grows, indicating a temporary rise in the uncertainty associated with the inactivity periods of the system components. This initial increase can be attributed to the overlapping or near-simultaneous inactive periods of multiple components, which momentarily intensify the overall uncertainty. After reaching a local maximum around $t \approx 2.5$, the extropy begins to decline and eventually stabilizes. This subsequent decrease and stabilization reflect the fact that, as time progresses, the inactivity periods become more predictable, leading to a reduction in uncertainty within the system.

Example 2 *Consider a coherent system characterized by the signature vector* $\boldsymbol{s} = (0, \ldots, 0, 1)$ *consisting of n statistically IID components. Each component lifetime follows a Weibull distribution with PDF* $g(y) = \frac{\alpha}{\lambda}\left(\frac{y}{\lambda}\right)^{\alpha-1}\exp\left[-\left(\frac{y}{\lambda}\right)^{\alpha}\right],\ y > 0.$. *In this example the system is a parallel system. For a parallel system the system remains operational as long as at least one component is alive; hence, the system lifetime is the maximum of component lifetimes, i.e.,* $T = \max\{Y_1, \ldots, Y_n\} = Y_{n:n}$. *With this signature, we have* $P(T = Y_{k:n}) = 0$ *for* $k = 1, 2, \ldots, n-1$, *meaning that none of the smaller order statistics can cause system failure. Therefore, when the system is still functioning at an observation time* $t > 0$ *(i.e.,* $T > t$*), it is possible that several components have already failed, i.e.,* $Y_{k:n} < t$ *for some* $k < n$. *In this setting, the conditional random variable of interest is the inactivity time of such failed components, defined by* $t - Y_{k:n} \mid \left(T > t,\, Y_{k:n} < t\right)$ *for* $k = 1, \ldots, n-1$. *This variable represents the elapsed time since the failure of the k-th order component up to the observation epoch t, given that the system is still alive at time t. The general functional associated with the inactivity-time process is expressed, following Equation* (10) *for* $j = n-2$, $\lambda = 1.5$, *and* $\alpha = 0.5$, *as*

$$\begin{aligned} J(IT_{n-2,n}(t)) &= -\frac{1}{2}(n-2)^2\Bigg[\frac{(n(n-1)/2)^2}{\left(n(n-1)/2 + n(e^{(t/1.5)^{0.5}} - 1)\right)^2(2n-5)} \\ &+ \frac{2(n(n-1)/2)(n-1)n(e^{(t/1.5)^{0.5}} - 1)}{\left(n(n-1)/2 + n(e^{(t/1.5)^{0.5}} - 1)\right)^2(2n-5)(2n-4)} \\ &+ \frac{2((n-1)n)^2(e^{(t/1.5)^{0.5}} - 1)^2}{\left(n(n-1)/2 + n(e^{(t/1.5)^{0.5}} - 1)\right)^2(2n-5)(2n-4)(2n-3)}\Bigg] \end{aligned} \tag{15}$$

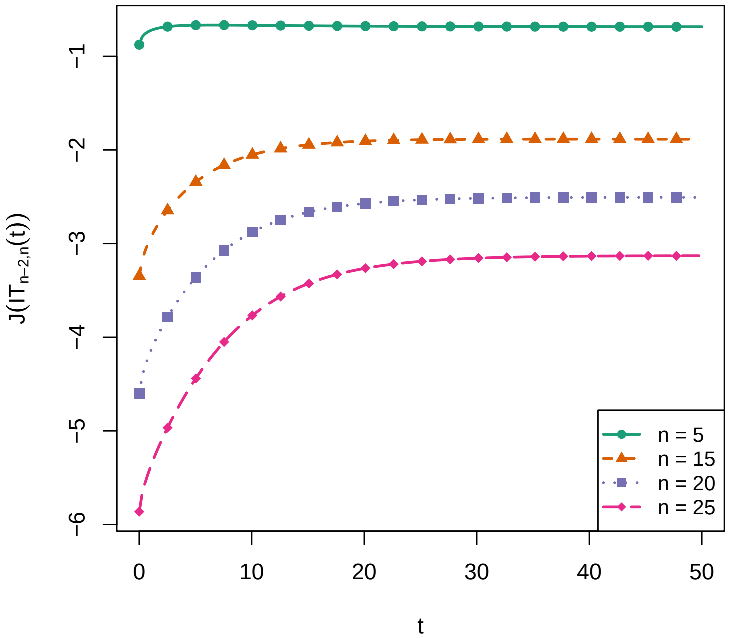

Figure 2: Behavior of $J(IT_{n-2,n}(t))$ as a function of t for different system sizes ($n = 5, 15, 20, 25$). The plot shows that extropy decreases as the number of components increases, reflecting higher uncertainty in the inactivity times of failed components of larger systems.

Figure 2 depicts the temporal evolution of the function $J(IT_{n-2,n}(t))$ for systems of various sizes, namely $n = 5, 15, 20,$ and 25. This measure captures the degree of uncertainty associated with system behavior, where smaller (more negative) values of $J(IT_{n-2,n}(t))$ imply greater ambiguity in identifying failed components. As the system size n grows, $J(IT_{n-2,n}(t))$ consistently attains lower values, revealing that larger systems experience higher uncertainty. This tendency arises because, in extensive systems, each failure leaves many components still active, whose potential inactivity spans a wider range of durations, thereby dispersing the probability mass more broadly. Consequently, $J(IT_{n-2,n}(t))$ becomes increasingly negative, mirroring heightened unpredictability. Over time, the curves show a monotonic decline of $J(IT_{n-2,n}(t))$, with their initial slope indicating how rapidly uncertainty accumulates. Smaller systems stabilize sooner at higher (less negative) levels, whereas larger systems descend more steeply, underscoring the pronounced amplification of uncertainty with system size.

In what follows, our objective is to establish a rigorous lower bound for the extropy measure associated with the inactivity times of failed components. This bound is formalized in the subsequent theorem, which expresses it in terms of the extropy corresponding to the inactivity times in an $(n - k + 1)$-out-of-n coherent system. Specifically, the formulation applies under the condition that the system remains operational at time t, while the component characterized by the lifetime $X_{k:n}$ has experienced failure at some instant prior to t, with k ranging from 1 to i.

Theorem 1 *Let $J(IT_{j,n}(t))$ denote the Extropy of the inactivity times of failed components, corresponding to the model function $\mathcal{M}_{IT_{j,n}(t),IY_{j,k,n}(t),IY^t_{l-j+1:l},\boldsymbol{q}(t),Y,G}$. Then, the following inequality holds*

$$J(IT_{j,n}(t)) \geq \sum_{r=i}^{n} q_r(t) J(IY_{j,r,n}(t)), \tag{16}$$

where, $IY_{j,r,n}(t)$ is the inactivity time of failed components in an $(n-r+1)$-out-of-n system with uniformly distributed components, when the system is working at time t and the component with lifetime $X_{k:n}$ has failed sometime before t for $k=1,\ldots,i$.

Proof. Invoking Jensen's inequality on equation (10) allows us to derive

$$\begin{aligned} J(IT_{j,n}(t)) &\geq -\frac{1}{2}\sum_{r=i}^{n} q_r(t)\int_0^\infty \left(g_{IY_{j,r,n}(t)}(y)\right)^2 dy \\ &= \sum_{r=i}^{n} q_r(t) J(IY_{j,r,n}(t)). \end{aligned}$$

Equality is realized in a $(n-k+1)$-out-of-n systems scenario, as the weighting function assigns $q_r(t)=0$ for all r not equal to $(n-k+1)$ and $q_r(t)=1$ when $r=n-k+1$. □

The following theorem provides an upper bound for the extropy of the inactivity times of failed components in the coherent system, expressed in terms of the weighted sum of the extropy of the shifted inactivity variables $IY^t_{l-j+1:l}$, with weights determined by $q_k(t)B_{l,j,k,n}(t)$.

Theorem 2 *Let $J(IT_{j,n}(t))$ denote the extropy of the inactivity times of failed components with the corresponding model function $\mathcal{M}_{IT_{j,n}(t),IY_{j,k,n}(t),IY^t_{l-j+1:l},\boldsymbol{q}(t),Y,G}$. Then*

$$J(IT_{j,n}(t)) \geq \sum_{k=i}^{n}\sum_{l=j}^{k-1} q_k(t) B_{l,j,k,n}(t) J(IY^t_{l-j+1:l}). \tag{17}$$

Proof. Through the application of Jensen's inequality to equation (10), the following result is obtained

$$\begin{aligned} J(IT_{j,n}(t)) &\geq -\frac{1}{2}\sum_{k=i}^{n}\sum_{l=j}^{k-1} q_k(t) B_{l,j,k,n}(t)\int_0^\infty \left(g_{IY^t_{l-j+1:l}}(y)\right)^2 dy \\ &= \sum_{k=i}^{n}\sum_{l=j}^{k-1} q_k(t) B_{l,j,k,n}(t) J(IY^t_{l-j+1:l}). \end{aligned}$$

□

In the example below, we analyze and compare the lower bounds provided by Theorems 1 and 2.

Example 3 *Consider a coherent system characterized by the signature vector* $\boldsymbol{s} = \left(0, \frac{1}{3}, \frac{5}{12}, \frac{1}{4}\right)$, *which consists of four statistically IID components. Each component lifetime follows a Weibull distribution with shape parameter* $\alpha = 0.8$ *and scale parameter* $\lambda = 3$, *having PDF* $g(y) = \frac{\alpha}{\lambda}\left(\frac{y}{\lambda}\right)^{\alpha-1} e^{-(y/\lambda)^{\alpha}}, \quad y > 0$, *and CDF* $G(y) = 1 - e^{-(y/\lambda)^{\alpha}}, \quad y > 0$. *After carrying out the calculations, the lower bounds stated in Theorems 1 and 2 are obtained in Figure 6. In Figure 6, we illustrate the extropy function* $J(IT_{2,4}(t))$ *together with the lower bounds derived in Theorems 1 and 2. The first lower bound, derived from Theorem 1, is denoted by* $L_1(t)$, *whereas the second lower bound, established in Theorem 2, is represented by* $L_2(t)$. *As shown in the Figure 6, the extropy function* $J(IT_{2,4}(t))$ *decreases smoothly with time* t. *Both bounds provide conservative approximations, but* $L_1(t)$ *lies consistently closer to the true extropy curve, indicating that the bound derived in Theorem 1 is sharper than the one obtained in Theorem 2.*

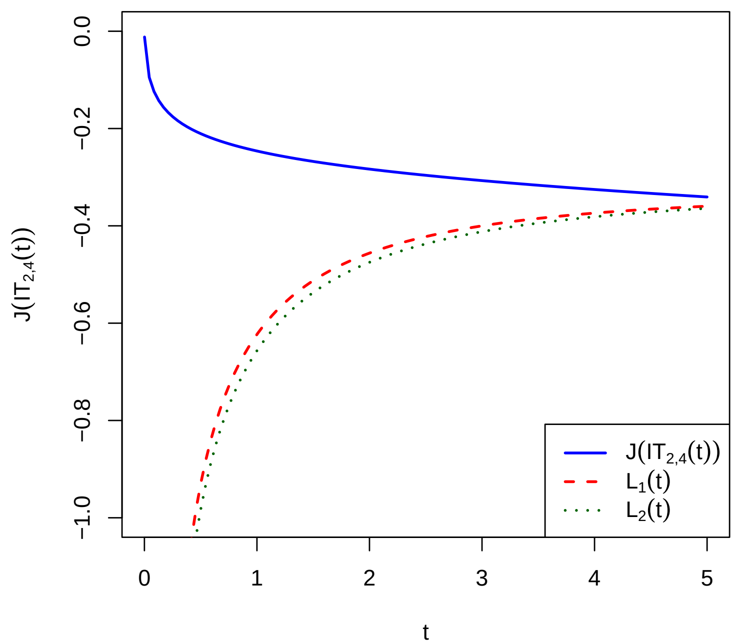

Figure 3: Comparison of the two lower bounds, $L_1(t)$ and $L_2(t)$, for the extropy of the inactivity times failed components in systems with Weibull-distributed component lifetimes. The results indicate that $L_1(t)$ consistently lies closer to the exact extropy values, thereby providing a sharper and more accurate approximation than $L_2(t)$.

3 Coherent systems of four Weibull distributed components with the signature vector $\boldsymbol{s} = (0, \ldots, 0, s_i, \ldots, s_n)$

This section delves into the extropy for the inactivity times of the failed components in a coherent system composed of n statistically IID units, where each component lifetime follows a Weibull distribution. The PDF and CDF of each component lifetime are given by $g_Y(y) =$

$\frac{k}{\lambda}\left(\frac{y}{\lambda}\right)^{k-1} e^{-(y/\lambda)^k}, \quad y > 0$, and $G_Y(y) = 1 - e^{-(y/\lambda)^k}$. In what follows, we consider coherent systems with signature vectors of the form $\boldsymbol{s} = (0, \ldots, 0, s_i, \ldots, s_n)$ for $1 < i \leq n$, so that only the order statistics $X_{k:n}$ with $k > i$ may represent the system's failure time. Equivalently, $P(T = X_{k:n}) = 0, \quad k = 1, 2, \ldots, i$, which means that the early lifetimes $X_{1:n}, \ldots, X_{i:n}$ cannot trigger system failure. As a result, when the system is still operational at time t (i.e., $T > t$), it is possible that these components have already failed before t, that is, $X_{k:n} < t$ for some $k \leq i$. For illustration, Table 1 presents several examples of four-component coherent systems characterized by their structure function $T(4)$ and the corresponding signature vectors of the form $\boldsymbol{s} = (0, \ldots, 0, s_i, \ldots, s_n)$.

Table 1: Representative examples of coherent systems with four components, described through the structure function $T(4)$ and their associated signature vectors in the form $\boldsymbol{s} = (0, \ldots, 0, s_i, \ldots, s_n)$.

System	$T = \phi(Y_1, Y_2, Y_3, Y_4)$	**Signature**
1	$Y_{2:2} = \max(Y_1, Y_2)$ (2-parallel)	$\left(0, \frac{1}{6}, \frac{1}{3}, \frac{1}{2}\right)$
2	$\max(Y_2, \min(Y_1, Y_3))$ (consecutive 2-out-of-3: F)	$\left(0, \frac{1}{3}, \frac{5}{12}, \frac{1}{4}\right)$
3	$\max(Y_1, \min(Y_2, Y_3, Y_4))$	$\left(0, \frac{1}{2}, \frac{1}{4}, \frac{1}{4}\right)$
4	$\max(Y_1, \min(Y_2, Y_3), \min(Y_3, Y_4))$ (3-parallel)	$\left(0, \frac{1}{6}, \frac{7}{12}, \frac{1}{4}\right)$
5	$\max(Y_1, Y_2, Y_3)$	$\left(0, 0, \frac{1}{4}, \frac{3}{4}\right)$
6	$\max(Y_{2:3}, Y_4)$	$\left(0, 0, \frac{3}{4}, \frac{1}{4}\right)$
7	$\min(\max(Y_1, Y_2, Y_3), \max(Y_2, Y_3, Y_4))$ (consecutive 3-out-of-4: F)	$\left(0, 0, \frac{1}{2}, \frac{1}{2}\right)$
8	$Y_{4:4} = \max(Y_1, Y_2, Y_3, Y_4)$ (parallel)	$(0, 0, 0, 1)$

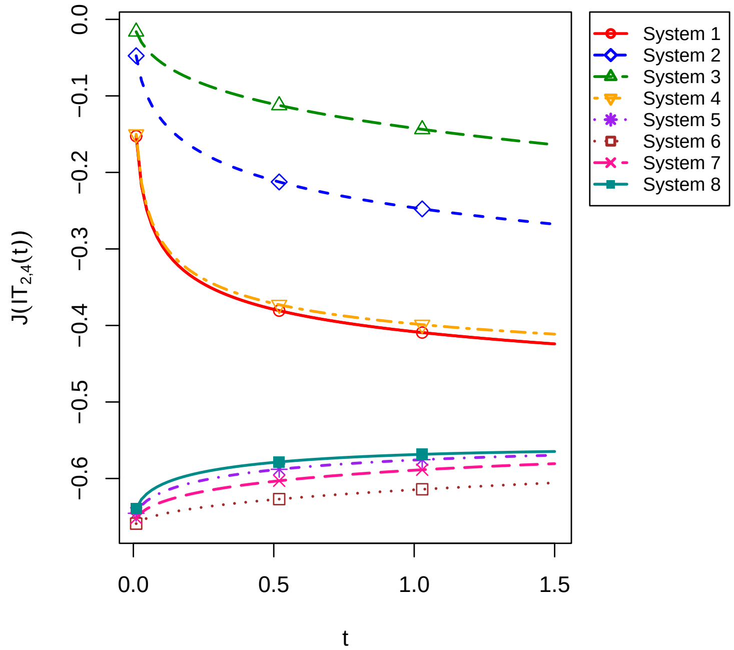

Figure 4: Variation of $J(IT_{2,4}(t))$ for the eight coherent systems listed in Table 1, obtained under a Weibull lifetime model with shape parameter $k = 0.4$ and scale parameter $\lambda = 1.5$. The results indicate that System 6 attains the smallest $J(IT_{1,4}(t))$ values, representing the highest degree of structural uncertainty, while System 3 achieves the largest $\xi J(IT_{1,4}(t))$ values, corresponding to the most reliable and least uncertain configuration among the examined systems.

Figure 5 illustrates the evolution of the uncertainty measure $J(IT_{2,4}(t))$ for the inactivity times of failed components in eight coherent systems characterized by distinct signature vectors, under a Weibull model with parameters $\alpha = 0.4$ and $\lambda = 1.5$. This measure reflects the dynamic uncertainty associated with the residual inactivity of failed components, where larger (less negative) values of $J(IT_{2,4}(t))$ indicate greater predictability and structural stability.

At small values of t, the systems exhibit similar trends; however, as time progresses, clear distinctions emerge among their reliability patterns. System 3 (green curve) consistently maintains the highest $J(IT_{2,4}(t))$ values, signifying the lowest level of uncertainty and the most robust reliability performance throughout the observation horizon. This indicates that the inactivity periods of failed components in System 3 are highly predictable, reflecting its superior structural configuration.

In contrast, System 6 (brown curve) shows the lowest $J(IT_{2,4}(t))$ values, implying the highest uncertainty and the most erratic behavior in the inactivity times. Systems 5, 7, and 8 follow closely in the lower range of $J(IT_{2,4}(t))$, suggesting comparably unstable reliability structures. Systems 1 and 4 occupy intermediate positions, displaying moderate uncertainty levels, while System 2 ranks just below System 3, indicating relatively high stability and reliability.

Overall, the systems can be ranked from *highest to lowest uncertainty* (i.e., from smallest to largest $J(IT_{2,4}(t))$) as follows:

System 6 $>$ System 8 $>$ System 5 $>$ System 7 $\approx$ System 1 $>$ System 4 $>$ System 2 $>$ System 3.

This comparative analysis demonstrates that the $J(IT_{2,4}(t))$ measure provides a sensitive and discriminating framework for evaluating system-level uncertainty. Systems with smaller $J(IT_{2,4}(t))$ values experience higher unpredictability in component inactivity and thus demand more frequent inspection and preventive maintenance, whereas those with larger values, particularly System 3 exhibit enhanced reliability and structural robustness, allowing for more flexible maintenance strategies and longer operational lifetimes.

4 Non-parametric Estimators for $J(IT_{j,n}(t))$

In this section, two non-parametric estimators are proposed: a plug-in estimator, and a kernel-smoothed log-odds estimator. Let $R(t) = \frac{G(t)}{\bar{G}(t)}$. For a random sample $X_1, \ldots, X_N$, let the empirical estimator of the CDF be

$$\widehat{G}(t) = \frac{1}{N} \sum_{r=1}^{N} \mathbf{1}\{X_r \leq t\}, \qquad \widehat{\bar{G}}(t) = 1 - \widehat{G}(t),$$

Define the empirical odds

$$\widehat{R}_{\text{plug}}(t) = \frac{\widehat{G}(t)}{\max\{1 - \widehat{G}(t),\, \varepsilon\}}, \quad \varepsilon > 0.$$

Then replace $R(t)$ by $\widehat{R}_{\text{plug}}(t)$ in (4) and (5) to obtain

$$\widehat{q}_k(t) = \frac{s_k \displaystyle\sum_{l=j}^{k-1} \binom{n}{l} \widehat{R}_{\text{plug}}(t)^l}{\displaystyle\sum_{m=i}^{n} \sum_{l=j}^{m-1} s_m \binom{n}{l} \widehat{R}_{\text{plug}}(t)^l},$$

and

$$\widehat{B}_{l,j,k,n}(t) = \frac{\binom{n}{l} \widehat{R}_{\text{plug}}(t)^l}{\displaystyle\sum_{r=j}^{k-1} \binom{n}{r} \widehat{R}_{\text{plug}}(t)^r}.$$

The plug-in estimator is

$$\widehat{J}_{\text{plug}}(t) = -\frac{1}{2} \int_0^1 \left[\sum_{k=i}^{n} \sum_{l=j}^{k-1} \widehat{q}_k(t)\, \widehat{B}_{l,j,k,n}(t)\, j \binom{l}{j} (1-u)^{j-1} u^{l-j} \right]^2 du. \tag{18}$$

The integral is evaluated numerically using a trapezoid or Gauss-Legendre rule over a uniform grid $u_m \in [0,1]$.

Algorithm 1 Plug-in Estimator of $J(IT_{j,n}(t))$

Choose a grid $\{u_m\}_{m=1}^{M} \subset [0,1]$ and small $\varepsilon > 0$.
Compute $\widehat{G}(t) = \frac{1}{N}\sum 1\{X_i \le t\}$ (or $1 - \widehat{S}_{\mathrm{KM}}(t)$ if censored).
Set $\widehat{R}_{\mathrm{plug}}(t) = \widehat{G}(t)/\max\{1-\widehat{G}(t), \varepsilon\}$.
for $k = i$ to n **do**
    $\widehat{q}_k(t) = \dfrac{s_k \sum_{l=j}^{k-1} \binom{n}{l} \widehat{R}_{\mathrm{plug}}(t)^l}{\sum_{m=i}^{n}\sum_{l=j}^{m-1} s_m \binom{n}{l} \widehat{R}_{\mathrm{plug}}(t)^l}$.
    for $l = j$ to $k-1$ **do**
        $\widehat{B}_{l,j,k,n}(t) = \dfrac{\binom{n}{l} \widehat{R}_{\mathrm{plug}}(t)^l}{\sum_{r=j}^{k-1} \binom{n}{r} \widehat{R}_{\mathrm{plug}}(t)^r}$.
    end for
end for
For each u_m, compute $A(u_m;t) = \displaystyle\sum_{k=i}^{n}\sum_{l=j}^{k-1} \widehat{q}_k(t)\, \widehat{B}_{l,j,k,n}(t)\, j \binom{l}{j} (1-u_m)^{j-1} u_m^{l-j}$.
Approximate $\widehat{J}_{\mathrm{plug}}(t) = -\frac{1}{2}\displaystyle\sum_{m=1}^{M-1} \frac{u_{m+1}-u_m}{2}\left[A(u_m;t)^2 + A(u_{m+1};t)^2\right]$.

To reduce the variability of the empirical CDF near 0 or 1, a smooth CDF estimator is used. Let $K(\cdot)$ be a smooth cumulative kernel (e.g. the standard normal CDF) and let $h > 0$ be a bandwidth. Define

$$\widehat{G}_h(t) = \frac{1}{N}\sum_{r=1}^{N} K\left(\frac{t - X_r}{h}\right),$$

and

$$\widehat{R}_{\mathrm{kerlog}}(t) = \frac{\widehat{G}_h(t)}{1 - \widehat{G}_h(t)}.$$

Replace $R(t)$ by $\widehat{R}_{\mathrm{kerlog}}(t)$ in (4) and (5) and evaluate

$$\widehat{J}_{\mathrm{kerlog}}(t) = -\frac{1}{2}\int_0^1 \left[\sum_{k=i}^{n}\sum_{l=j}^{k-1} \widehat{q}_k^{(\mathrm{ker})}(t)\, \widehat{B}_{l,j,k,n}^{(\mathrm{ker})}(t)\, j \binom{l}{j} (1-u)^{j-1} u^{l-j}\right]^2 du. \tag{19}$$

Algorithm 2 Kernel-Logit Estimator of $J(IT_{j,n}(t))$

1: Choose kernel $K(\cdot)$ (e.g. normal CDF) and bandwidth h.
2: Compute $\widehat{G}_h(t) = \frac{1}{N}\sum K((t - X_i)/h)$.
3: Clip $\widehat{G}_h(t)$ to $[\varepsilon, 1-\varepsilon]$ and compute $\widehat{R}_{\text{kerlog}}(t) = \widehat{G}_h(t)/(1 - \widehat{G}_h(t))$.
4: Replace $R(t)$ by $\widehat{R}_{\text{kerlog}}(t)$ in the definitions of $q_k(t)$ and $B_{l,j,k,n}(t)$.
5: Evaluate the double sum inside the square brackets of (19) for each u_m and compute the integral numerically.
6: Return $\widehat{J}_{\text{kerlog}}(t)$.

To evaluate the performance of the proposed non-parametric estimators, a simulation study is conducted for the following distributions:

1. Weibull distribution with shape parameter $k = 0.5$ and scale $\lambda = 1.5$:

$$F(x) = 1 - e^{-(x/1.5)^{0.5}}, \quad x > 0$$

2. Gamma distribution with shape parameter $k = 2$ and scale $\lambda = 1.5$:

$$F(x) = \frac{1}{\Gamma(2)}\,\gamma\Big(2, \frac{x}{1.5}\Big), \quad x > 0$$

where $\gamma(k, x) = \int_0^x t^{k-1}e^{-t}dt$ is the lower incomplete gamma function.

3. Exponential distribution with rate parameter $\lambda = 1.5$:

$$F(x) = 1 - e^{-1.5x}, \quad x > 0$$

4. Pareto distribution with shape parameter $\alpha = 2$ and scale $x_m = 1.5$:

$$F(x) = 1 - \Big(\frac{1.5}{x}\Big)^2, \quad x \geq 1.5$$

For each distribution, the average bias and root mean square error (RMSE) of the plug-in and kernel-logit estimators of $J(IT_{j,n}(t))$ are computed for various sample sizes $N = 20, 30, 50, 100$ and different system sizes n. The smoothing parameter h for the kernel-based estimator is selected using the heuristic formula $h = \lfloor\sqrt{N} + 0.5\rfloor$, where $\lfloor\cdot\rfloor$ denotes the integer part.

Each simulation is repeated over 5,000 iterations for $j = n-2$ and $\boldsymbol{s} = (0, \ldots, 0, 1)$. The results, presented in Tables 2,3,4, and 5 show that as the sample size increases, the RMSE decreases, while the bias tends to increase slightly. These trends are observed consistently across all considered distributions.

Table 2: Comparison of nonparametric estimators of $J(IT_{j,n}(2))$ for Weibull($k = 0.5, \lambda = 1.5$)

n_{sys}	N_{sample}	Plug-in		Kerlog	
		Bias	RMSE	Bias	RMSE
5	20	-0.00086	0.02064	-0.00149	0.01987
5	30	-0.00378	0.01906	-0.00404	0.01832
5	50	-0.00312	0.01643	-0.00324	0.01573
5	100	-0.00052	0.01057	-0.00094	0.01057
7	20	-0.00549	0.05835	-0.00694	0.05537
7	30	0.00090	0.05749	0.00070	0.05612
7	50	-0.00042	0.04166	-0.00144	0.03971
7	100	0.00070	0.03178	-0.00148	0.03137
10	20	0.00580	0.11947	0.00308	0.11879
10	30	0.00179	0.10592	-0.00181	0.10083
10	50	0.00084	0.07872	0.00017	0.07632
10	100	0.00549	0.05839	0.00024	0.05634
15	20	0.02727	0.20715	0.02036	0.19422
15	30	0.01038	0.13987	0.00339	0.13124
15	50	0.00893	0.12972	0.00330	0.12327
15	100	0.02127	0.09456	0.01565	0.09012

For the Weibull distribution with shape parameter $k = 0.5$ and scale $\lambda = 1.5$, both the plug-in and kernel-logit estimators demonstrate satisfactory performance across all sample sizes. The bias of both estimators remains close to zero, indicating accurate estimation of $J(IT_{j,n}(t))$. However, the kernel-logit estimator consistently exhibits slightly lower RMSE values, particularly for smaller sample sizes, suggesting a more stable estimation in the presence of limited data. This trend highlights the advantage of the kernel-based smoothing in reducing variability without introducing significant bias (see Table 2).

Table 3: Comparison of nonparametric estimators of $J(IT_{j,n}(2))$ for Gamma($k = 2, \lambda = 1.5$)

n_{sys}	N_{sample}	Plug-in		Kerlog	
		Bias	RMSE	Bias	RMSE
5	20	-0.00220	0.03397	-0.00151	0.02964
5	30	0.00247	0.02822	0.00177	0.02434
5	50	-0.00533	0.02195	-0.00499	0.02041
5	100	-0.00145	0.01497	-0.00197	0.01395
7	20	-0.00785	0.05464	-0.00816	0.04921
7	30	-0.00160	0.04481	-0.00162	0.04078
7	50	0.00466	0.03949	0.00267	0.03537
7	100	-0.00240	0.02570	-0.00216	0.02382
10	20	0.00056	0.07841	-0.00317	0.06930
10	30	0.00286	0.06390	0.00318	0.05797
10	50	0.00789	0.05495	0.00666	0.05038
10	100	0.00294	0.03796	0.00098	0.03471
15	20	0.02552	0.11258	0.02194	0.10375
15	30	0.00587	0.08562	0.00041	0.07936
15	50	0.00493	0.07530	0.00348	0.07064
15	100	0.00369	0.04620	0.00233	0.04101

For the Gamma distribution with shape $k = 2$ and scale $\lambda = 1.5$, a similar pattern is observed. While the biases of both estimators are generally small, the kernel-logit estimator tends to provide a slightly lower RMSE for most sample sizes, especially when N is small or moderate. These results indicate that kernel smoothing effectively enhances estimator performance by controlling random fluctuations in the empirical CDF, leading to more reliable estimates of $J(IT_{j,n}(t))$ (see Table 3).

Table 4: Comparison of nonparametric estimators of $J(IT_{j,n}(2))$ for Exponential($\lambda = 1.5$)

n_{sys}	N_{sample}	Plug-in		Kerlog	
		Bias	RMSE	Bias	RMSE
5	20	-0.00361	0.00853	-0.00195	0.00703
5	30	-0.00087	0.00599	0.00028	0.00485
5	50	-0.00120	0.00504	0.00004	0.00413
5	100	-0.00033	0.00360	0.00041	0.00311
7	20	-0.00780	0.01315	-0.00715	0.01236
7	30	-0.00682	0.01138	-0.00586	0.01089
7	50	-0.00366	0.00637	-0.00257	0.00493
7	100	-0.00157	0.00292	-0.00180	0.00342
10	20	-0.02116	0.04937	-0.01953	0.04429
10	30	-0.01048	0.03667	-0.01229	0.03827
10	50	-0.00527	0.02060	-0.00737	0.02202
10	100	-0.00582	0.01827	-0.00951	0.02004
15	20	-0.03681	0.13873	-0.04245	0.13533
15	30	-0.02090	0.11396	-0.02694	0.10861
15	50	-0.00216	0.07754	-0.01329	0.07142
15	100	-0.01809	0.07900	-0.02493	0.07326

In the case of the Exponential distribution with rate $\lambda = 1.5$, the performance of both estimators is again comparable, with bias values near zero. The kernel-logit estimator achieves marginally lower RMSEs across most sample sizes, demonstrating its ability to provide slightly more precise estimates in small samples. The differences between the two estimators diminish as the sample size increases, reflecting the convergence properties of the plug-in approach with large datasets (see Table 4).

Table 5: Comparison of nonparametric estimators of $J(IT_{j,n}(2))$ for Pareto($\alpha = 2$, $x_m = 1.5$)

n_{sys}	N_{sample}	Plug-in		Kerlog	
		Bias	RMSE	Bias	RMSE
5	20	-0.00184	0.03402	-0.01142	0.02780
5	30	0.00013	0.02957	-0.00785	0.02304
5	50	-0.00120	0.02188	-0.01108	0.02004
5	100	-0.00188	0.01748	-0.01132	0.01764
7	20	0.00702	0.05024	-0.01182	0.04027
7	30	0.00339	0.05210	-0.01914	0.04227
7	50	0.00025	0.03981	-0.01882	0.03555
7	100	0.00019	0.02738	-0.01871	0.02780
10	20	0.00629	0.09182	-0.02061	0.07030
10	30	0.00539	0.07527	-0.01900	0.05961
10	50	0.00487	0.06270	-0.02288	0.04774
10	100	-0.00137	0.03907	-0.02781	0.04068
15	20	0.01109	0.12042	-0.02524	0.08370
15	30	0.01962	0.09127	-0.02305	0.05936
15	50	0.00560	0.07622	-0.02656	0.06007
15	100	-0.00527	0.04510	-0.03656	0.04816

For the Pareto distribution with shape $\alpha = 2$ and scale $x_m = 1.5$, the behavior differs slightly. While both estimators remain reasonably accurate, the plug-in estimator often exhibits a lower RMSE than the kernel-logit estimator for larger sample sizes, despite comparable bias levels. This suggests that for heavy-tailed distributions, the plug-in approach may offer slightly more stable performance, whereas kernel smoothing may introduce additional variability in the tails. Overall, the simulation results demonstrate that both estimators perform well, with kernel-logit generally preferable for light- to moderate-tailed distributions and plug-in slightly advantageous for heavy-tailed distributions (see Table 5).

4.1 Consistency and equivariance results for $J(IT_{j,n}(t))$

We study the functional

$$J\big(IT_{j,n}(t);R\big) = -\frac{1}{2}\int_0^1 \left(\sum_{k=i}^{n}\sum_{l=j}^{k-1} q_k(R)\, B_{l,j,k,n}(R)\; j\binom{l}{j}(1-u)^{j-1}u^{\,l-j} \right)^2 du,$$

where for a given odds function $R > 0$ the coefficients are defined (whenever denominators are non-zero) by

$$q_k(R) = \frac{s_k \displaystyle\sum_{l=j}^{k-1}\binom{n}{l}R^l}{\displaystyle\sum_{m=i}^{n} s_m \sum_{l=j}^{m-1}\binom{n}{l}R^l}, \qquad B_{l,j,k,n}(R) = \frac{\binom{n}{l}R^l}{\displaystyle\sum_{r=j}^{k-1}\binom{n}{r}R^r}.$$

We assume the weight vector $s = (s_1, \dots, s_n)$ is fixed and that for the evaluation point t the true CDF satisfies $0 < G(t) < 1$. Standard measurability (continuity) conditions for the finite sums below are then satisfied.

Theorem 3 (Strong consistency of the plug-in estimator) *Let $X_1, \dots, X_N$ be IID with CDF G. Fix n, i, j as above and a point t with $0 < G(t) < 1$. Define $\widehat{G}_N(t) = \frac{1}{N}\sum_{m=1}^{N}\mathbf{1}\{X_m \le t\}$, $\widehat{R}_N(t) = \frac{\widehat{G}_N(t)}{1-\widehat{G}_N(t)}$, and the plug–in estimator $\widehat{J}_{N,\mathrm{plug}}(t) = J(IT_{j,n}(t); \widehat{R}_N(t))$. Then*

$$\widehat{J}_{N,\mathrm{plug}}(t) \xrightarrow{\text{a.s.}} J(IT_{j,n}(t); R(t)) \quad \text{as } N \to \infty, \tag{20}$$

where $R(t) = G(t)/(1 - G(t))$.

Proof. We first note that by the Strong Law of Large Numbers (SLLN) applied to the indicator function at the fixed point t, we have $\widehat{G}_N(t) \to G(t)$ almost surely (see e.g. Billingsley (1995) or Feller for the classical SLLN). Because $0 < G(t) < 1$ and $\widehat{G}_N(t) \in [0, 1]$ almost surely, we may apply the continuous mapping theorem (see van der Vaart (1998), Theorem 1.3.6) to the continuous function $x \mapsto x/(1-x)$ on a neighborhood of $G(t)$; this gives $\widehat{R}_N(t) \to R(t)$ almost surely.

Next, consider the inner summand

$$A(u;R) = \sum_{k=i}^{n}\sum_{l=j}^{k-1} q_k(R)\, B_{l,j,k,n}(R)\; j\binom{l}{j}(1-u)^{j-1}u^{\,l-j},$$

viewed as a function of $(u, R) \in [0, 1] \times (0, \infty)$. Each coefficient $q_k(R)$ and $B_{l,j,k,n}(R)$ is a ratio of finite sums of continuous functions $R \mapsto R^l$ with strictly positive denominators for $R > 0$ (given the index ranges and non-negative binomial coefficients). Thus q_k and $B_{l,j,k,n}$ are continuous in R on $(0, \infty)$, and therefore $A(u; R)$ is continuous in (u, R). Since $[0, 1]$ is compact and the finite summation yields bounded integrands for R in a neighborhood of $R(t)$, the map $R \mapsto \int_0^1 A(u; R)^2 du$ is continuous by an application of the Dominated Convergence Theorem (DCT) or uniform continuity on compacta; see Folland (1999) or Royden for DCT. Concretely, for any sequence $R_n \to R$ we have $A(\cdot, R_n)^2 \to A(\cdot, R)^2$ pointwise and the integrands are uniformly bounded on $[0,1]$ by a finite constant determined by combinatorial coefficients and a neighborhood bound on R, so DCT yields convergence of integrals.

Combining the two convergence results: $\widehat{R}_N(t) \to R(t)$ a.s. and continuity of $R \mapsto J(IT_{j,n}(t); R)$ at $R(t)$, we obtain

$$\widehat{J}_{N,\text{plug}}(t) = J(IT_{j,n}(t); \widehat{R}_N(t)) \xrightarrow{\text{a.s.}} J(IT_{j,n}(t); R(t)),$$

as required. $\square$

Theorem 4 (Consistency of the kernel–logit estimator) *Under the setting of Theorem 1, assume additionally that $\mathbb{E}|X_1|^p < \infty$ for some $p > 1$. Let $h_N > 0$ be a bandwidth sequence with $h_N \downarrow 0$ and $Nh_N \to \infty$. Define the smoothed estimator*

$$\widehat{G}_{N,h}(t) = \frac{1}{N}\sum_{m=1}^{N} \Phi\Big(\frac{t - X_m}{h_N}\Big), \qquad \widehat{R}_{N,h}(t) = \frac{\widehat{G}_{N,h}(t)}{1 - \widehat{G}_{N,h}(t)},$$

and set $\widehat{J}_{N,\text{kerlog}}(t) = J(IT_{j,n}(t); \widehat{R}_{N,h}(t))$. Then for fixed t,

$$\widehat{J}_{N,\text{kerlog}}(t) \xrightarrow{p} J(IT_{j,n}(t); R(t)) \quad (N \to \infty).$$

If uniform a.s. convergence of $\widehat{G}_{N,h}$ holds under stronger regularity, the convergence may be strengthened to almost sure.

Proof. Kernel smoothing theory for distribution function estimators (see the discussion in Silverman (1986) and Wand & Jones (1995)) yields that under mild regularity—most importantly $h_N \to 0$ and $Nh_N \to \infty$—the smoothed estimator $\widehat{G}_{N,h}(t)$ is consistent for $G(t)$ in probability for each fixed t; the moment condition $\mathbb{E}|X_1|^p < \infty$ with $p > 1$ ensures control of boundary/bias terms and integrability required for the usual bias–variance analysis. Thus $\widehat{G}_{N,h}(t) \xrightarrow{p} G(t)$.

Applying the continuous mapping theorem (van der Vaart (1998)) to the continuous map $x \mapsto x/(1-x)$ gives $\widehat{R}_{N,h}(t) \xrightarrow{p} R(t)$. The remaining step is identical in spirit to the argument in Theorem 1: the functional $R \mapsto J(IT_{j,n}(t); R)$ is continuous at $R(t)$ because its integrand is jointly continuous in (u, R) and dominated on $[0,1]$ by an integrable bound for R near $R(t)$. Therefore, by another application of the continuous mapping theorem, we obtain $\widehat{J}_{N,\text{kerlog}}(t) = J(\widehat{R}_{N,h}(t)) \xrightarrow{p} J(R(t))$, as claimed. $\square$

Theorem 5 (Affine equivariance and moment identities) *Let $Y_i = cX_i + b$ with $c > 0$, $b \in \mathbb{R}$. Denote by G_X and G_Y the CDFs of X and Y, by R_X, R_Y their odds, and by $\widehat{J}_{m,X}, \widehat{J}_{m,Y}$ any* *plug-in–type estimators obtained by substituting an empirical or smoothed CDF into the functional J (this includes plug-in, kernel–logit, and leave-one-out jackknife versions). Then for each fixed t,*

$$J_Y(t) = J_X\Big(\frac{t-b}{c}\Big), \qquad \widehat{J}_{m,Y}(t) = \widehat{J}_{m,X}\Big(\frac{t-b}{c}\Big),$$

and consequently expectations, variances and RMSEs satisfy the corresponding identities:

$$\mathbb{E}[\widehat{J}_{m,Y}(t)] = \mathbb{E}\Big[\widehat{J}_{m,X}\Big(\frac{t-b}{c}\Big)\Big],$$

$$\mathrm{Var}(\widehat{J}_{m,Y}(t)) = \mathrm{Var}\Big(\widehat{J}_{m,X}\Big(\frac{t-b}{c}\Big)\Big), \quad \mathrm{RMSE}(\widehat{J}_{m,Y}(t)) = \mathrm{RMSE}\Big(\widehat{J}_{m,X}\Big(\frac{t-b}{c}\Big)\Big).$$

Proof. The identity $G_Y(t) = P(Y \le t) = P(X \le (t-b)/c) = G_X((t-b)/c)$ is immediate from the definition $Y = cX + b$. Consequently $R_Y(t) = R_X((t-b)/c)$ for each t. Because the functional J depends on the distribution only through the odds function R, it follows that $J_Y(t) = J_X((t-b)/c)$.

For estimators formed by substitution, plug-in versions satisfy exactly $\widehat{G}_{N,Y}(t) = \widehat{G}_{N,X}((t-b)/c)$ (empirical indicators transform accordingly), and the same relation holds for smoothed kernel versions after the natural bandwidth rescaling $h_Y = c\,h_X$ so that smoothing on the Y-scale corresponds to smoothing on the X-scale. Therefore $\widehat{R}_Y(\cdot) = \widehat{R}_X((\cdot - b)/c)$ and substituting into J yields $\widehat{J}_{m,Y}(t) = \widehat{J}_{m,X}((t-b)/c)$. The equalities of expectations, variances and RMSE then follow directly by taking expectation/variance of both sides (no asymptotic argument required). □

5 Image Processing Application Using the $J(IT_{j,n}(t))$ Measure

In this section, we demonstrate how the proposed estimator of $J(IT_{j,n}(t))$ can be applied to quantify structural uncertainty in digital images. Following the methodology of Toomaj and Atabay (2022) and Toomaj (2023), we begin with a normalized grayscale image denoted by X. In our experiment, X corresponds to a grayscale photograph of a cat. The image used in the image processing experiment is a publicly available photograph obtained from Wikimedia Commons (https://upload.wikimedia.org/wikipedia/commons/3/3a/Cat03.jpg). The original image is licensed for public use under the terms stated on its source page. We generate three modified versions of the image through deterministic intensity transformations:

$$Y = 0.9X + 0.1, \qquad Z = X^2, \qquad W = \sqrt{X}.$$

The transformation Y introduces a mild linear modification while largely preserving the contrast and structural information of the original image X. In contrast, Z applies a convex power transformation that amplifies bright intensities, whereas W, being a concave transformation, stretches low-intensity regions and generally leads to a loss of contrast and detail.

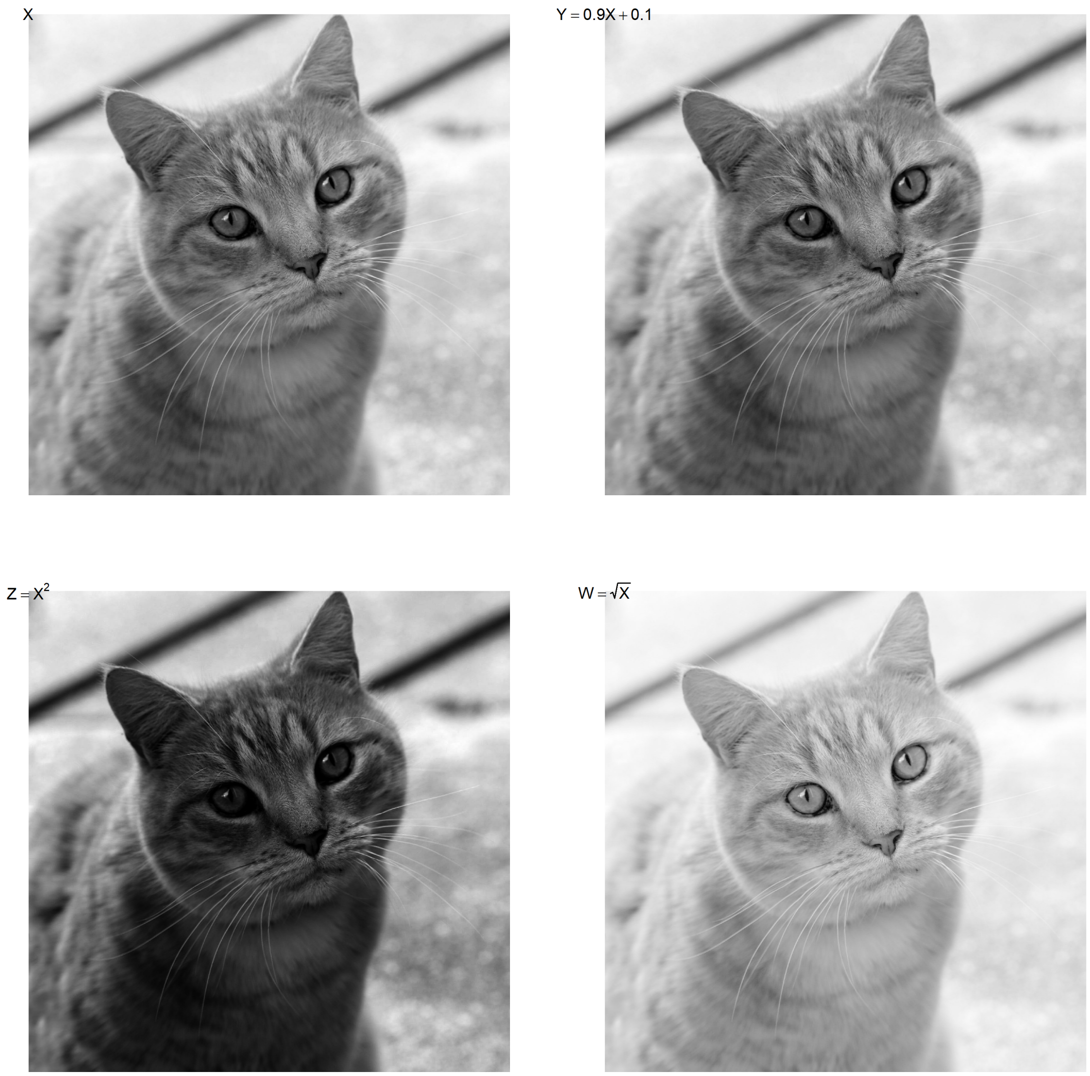

Figure 5: Sample picture of a cat with their adjustments

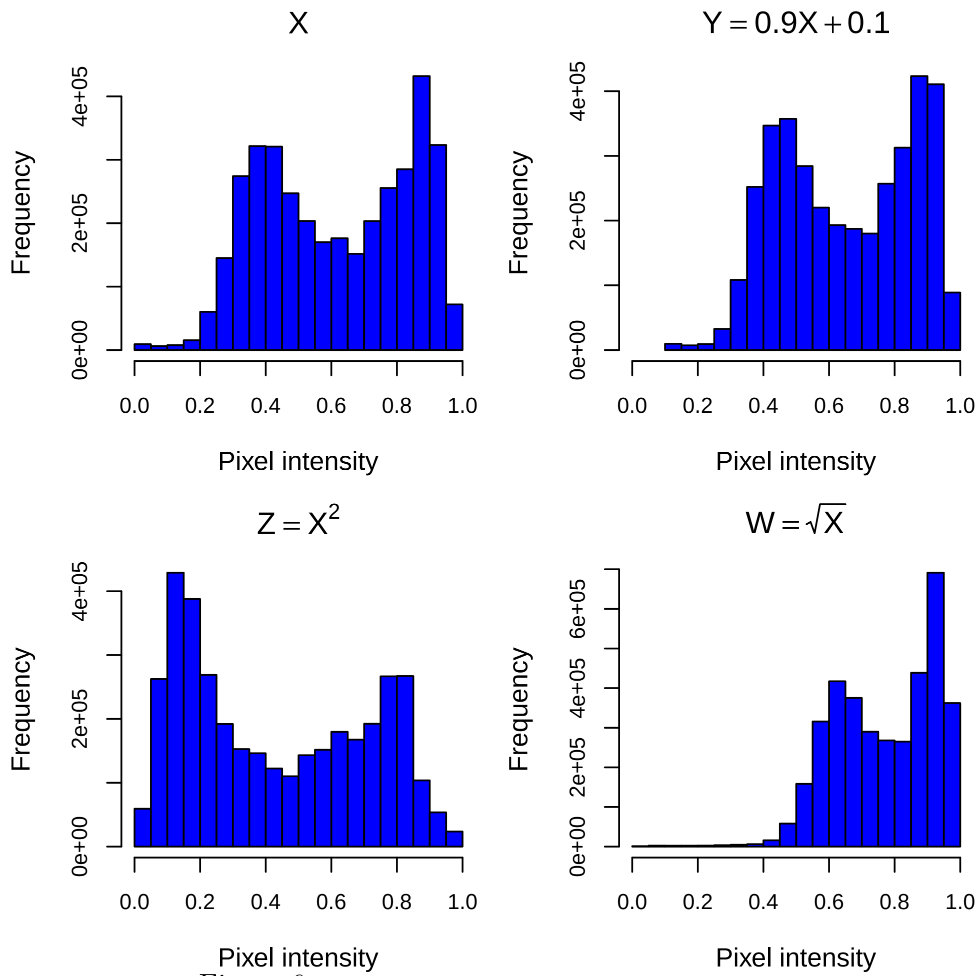

Figure 6: The histograms for pictures X, Y, Z and W.

For each image (X, Y, Z, W), we extract a random sample of pixel intensities and compute the plug-in and Kerlog estimators of $J(IT_{j,n}(t))$ on the grid $t \in [0, 0.8]$. The two sets of system parameters considered in this study are

$$n = 10, \quad i = 10, \quad j = 8, \quad \boldsymbol{s} = (0, \ldots, 0, 1),$$

and

$$n = 4, \quad i = 2, \quad j = 2, \quad \boldsymbol{s} = \left(0, \frac{1}{6}, \frac{7}{12}, \frac{1}{4}\right).$$

The corresponding estimators were then computed and their results are presented in Figures 7 and 8. The resulting measure $J(IT_{j,n}(t))$ contains information about the inactivity time distribution of a system constructed from the pixel intensity sample. Therefore, differences between the estimated curves provide a quantitative means to distinguish between structural changes introduced by different intensity transformations.

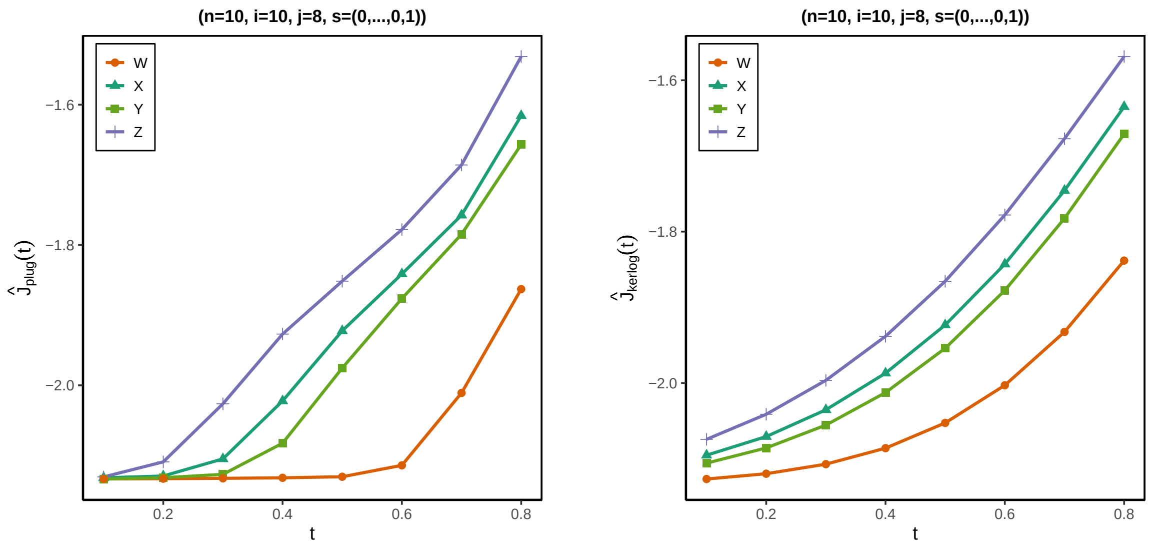

Figure 7: The values of estimators $\widehat{J}_{\text{kerlog}}(t)$ and $\widehat{J}_{\text{plug}}(t)$.

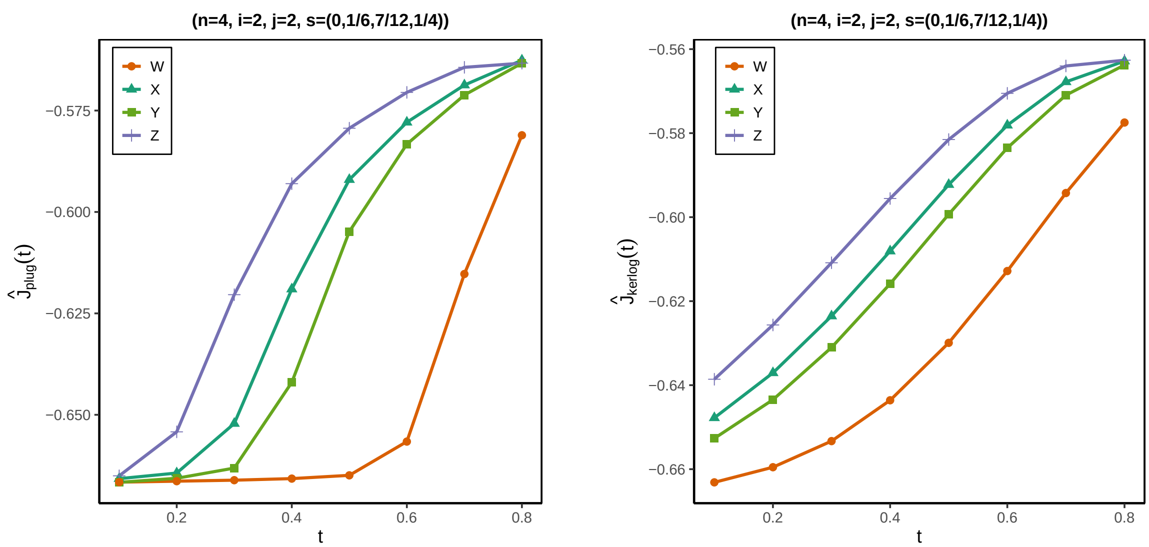

Figure 8: The values of estimators $\widehat{J}_{\text{kerlog}}(t)$ and $\widehat{J}_{\text{plug}}(t)$.

The estimated curves reveal a clear and consistent pattern. The curve associated with Y lies extremely close to that of the original image X, reflecting the fact that the transformation $Y = 0.9X + 0.1$ preserves the relative ordering of pixel intensities and leaves the overall distribution nearly unchanged.

The curve corresponding to $Z = X^2$ shows a moderate deviation from X, which is in line with the behavior of a convex power transformation that enhances bright regions more heavily than dark ones. Nonetheless, the structural relationship between Z and X remains relatively strong.

In contrast, the transformation $W = \sqrt{X}$ induces a substantial shift, and the estimated

$J(IT_{j,n}(t))$ curve diverges noticeably from those of X, Y, and Z for almost all t. This is expected, as the concave power transformation significantly flattens the intensity distribution and weakens structural dependencies.

These results show that the proposed estimator is sensitive to photometric distortions and captures distributional differences between images in a meaningful way. Transformations that preserve the monotonic structure of intensities (such as Y) produce curves close to the original image, while non-linear modifications (particularly W) generate clearly distinguishable deviation patterns.

Thus, the measure $J(IT_{j,n}(t))$ serves as a robust tool for assessing structural alterations in digital images and provides a principled, distribution-based method for quantifying image uncertainty.

6 Concluding Remarks

This paper provides a comprehensive investigation into the extropy associated with the inactivity times of failed components in coherent systems. By employing the system signature framework, we derived explicit representations for the extropy of inactivity durations and established several stochastic bounds and comparative results that reveal how system structure and configuration influence the informational characteristics of such hidden failure behavior. These theoretical developments offer a novel information-theoretic perspective on reliability analysis, complementing classical hazard-based and lifetime-based approaches that frequently overlook the latent contribution of failed components that persist within an otherwise functioning system.

On the methodological side, we introduced two non-parametric estimators for the extropy of inactivity times and examined their performance using simulated datasets under a variety of lifetime models. The numerical results demonstrate that both estimators provide reliable approximations, with the kernel-logit estimator showing superior performance for light- and medium-tailed distributions, whereas the plug-in estimator exhibits greater stability for heavy-tailed cases. These findings highlight the practical relevance of extropy-based measures in settings where the distributional behavior of inactivity times is complex or partially obscured.

Finally, the applicability of the proposed framework was illustrated through an image processing example, where extropy successfully captured subtle structural and contrast-related features under different intensity transformations. This demonstrates that the informational insights derived from extropy extend beyond classical reliability contexts and can be utilized in broader data-analytic and signal-processing environments. Overall, the results presented in this work emphasize the significance of inactivity times in understanding the hidden dynamics of coherent systems and underscore the potential of extropy as a powerful tool for both theoretical investigation and practical analysis.

Declarations

Ethics approval and consent to participate

This study does not involve human participants or animals. Therefore, ethical approval is not applicable.

Competing interests

The authors declare no competing interests.

Funding information

No funding was received for conducting this study.

Data Availability

The image used in the image-processing experiment is a publicly available photograph obtained from Wikimedia Commons (`https://upload.wikimedia.org/wikipedia/commons/3/3a/Cat03.jpg`). The original image is licensed for public use under the terms stated on its source page. The pixel–intensity samples employed in the numerical analysis, as well as the R code (file name: `CatPic.R`) used to generate the transformed images (file name: `Image_XYZW_Pixel_Samples.xls`) and compute the estimators, have been uploaded as supplementary materials on the manuscript's submission page. No additional datasets were generated or analysed in the current study.

Author Contributions

Zohreh Pakdaman and Reza Alizadeh Noughabi jointly developed the main theoretical framework, derived the mathematical results, and performed the analytical proofs. Both authors contributed equally to the writing of the manuscript, preparation of figures and numerical illustrations, and interpretation of the results. All authors reviewed and approved the final version of the manuscript. Both authors contributed equally to this work.

References

1. Belzunce, F., Riquelme, C. M., & Mulero, J. (2015). *An Introduction to Stochastic Orders.* Academic Press.

2. Billingsley, P. (1995). *Probability and Measure.* Wiley, New York.

3. Chakraborty, S., & Pradhan, B. (2022). Weighted cumulative residual Kullback–Leibler divergence: Properties and applications. *Communications in Statistics - Simulation and Computation*, **53**(7), 3541–3553.

4. Chakraborty, S., & Pradhan, B. (2023a). On estimation of cumulative residual extropy and its quantile version. *Ricerche di Matematica*, **74**(2), 1165–1176.

5. Chakraborty, S., & Pradhan, B. (2023b). Weighted negative cumulative extropy with application in testing uniformity. *Physica A: Statistical Mechanics and its Applications*, **612**, 128957.

6. Chakraborty, S., and Pradhan, B. (2024). On cumulative residual extropy of coherent and mixed systems. *Annals of Operations Research*, **340(1)**, 59–81.

7. Folland, G. B. (1999). *Real Analysis: Modern Techniques and Their Applications.* Wiley, New York.

8. Guo, Z., Zhang, J. and Yan, R. (2022). On inactivity times of failed components of coherent system under double monitoring. *Probability in the Engineering and Informational Sciences*, **36**(3), 923–940.

9. Goliforushani, S. and Asadi, M. (2011). Stochastic ordering among inactivity times of coherent systems. *Sankhya B*, **73**(2), 241–262.

10. Goliforushani, S., Asadi, M. and Balakrishnan, N. (2012). On the residual and inactivity times of the components of used coherent systems. *Journal of Applied Probability*, **49**(2), 385–404.

11. Jahanshahi, S. M. A., Zarei, H., and Khammar, A. H. (2020). On cumulative residual extropy. *Probability in the Engineering and Informational Sciences*, **34**(4), 605–625.

12. Jensen, J. L. W. V. (1906). Sur les fonctions convexes et les inégalités entre les valeurs moyennes. *Acta Mathematica*, **30**(1), 175–193.

13. Jose, J. and Sathar, E. A. (2019). Residual extropy of k-record values. *Statistics and Probability Letters*, **146**, 1–6.

14. Kayal, S. (2019). On a generalized entropy of mixed systems. *Journal of Statistics and Management Systems*, **22(6)**, 1183–1198.

15. Khaledi, B. E. and Shaked, M. (2007). Ordering conditional lifetimes of coherent systems. *Journal of Statistical Planning and Inference*, **137**, 1173–1184.

16. Kharazmi, O., and Balakrishnan, N. (2023). Cumulative and relative cumulative residual information generating measures and associated properties. *Communications in Statistics-Theory and Methods*, **52**(15), 5260–5273.

17. Kochar, S., Mukerjee, H. and Samaniego, F. J. (1999). The 'signature' of a coherent system and its application to comparisons among systems. *Naval Research Logistics*, **46**, 507–523.

18. Lad, F., Sanfilippo, G. and Agro, G. (2015). Extropy: Complementary dual of entropy. *Statistical Science*, **30**(1), 40–58.

19. Li, S. and Lynch, J. (2010). Some elementary ideas concerning the complexity of system structure. *Naval Research Logistics*, **57**, 626–633.

20. Li, X. and Zhao, P. (2008). Stochastic comparison on general inactivity time and general residual life of k-out-of-n systems. *Communications in Statistics-Simulation and Computation*, **37**(5), 1005–1019.

21. Navarro, J. and Hernandez, P. J. (2008). Mean residual life functions of finite mixtures, order statistics and coherent systems. *Metrika*, **67**, 277–298.

22. Navarro, J., Balakrishnan, N. and Samaniego, F. J. (2008). Mixture representations of residual lifetimes of used systems. *Journal of Applied Probability*, **45**, 1097–1112.

23. Navarro, J., Longobardi, M. and Pellerey, F. (2017). Comparison results for inactivity times of k-out-of-n and general coherent systems with dependent components. *Test*, **26**(4), 822–846.

24. Navarro, J. and Calì, C. (2019). Inactivity times of coherent systems with dependent components under periodical inspections. *Applied Stochastic Models in Business and Industry*, **35**(3), 871–892.

25. Pakdaman, Z. and Alizadeh Noughabi, R. (2025a). A new representation of some extropy-related measures based on probability density quantile. *International Journal of Reliability, Quality and Safety Engineering.*

26. Pakdaman, Z. and Noughabi, R. A. (2025b). On the study of the cumulative residual extropy of mixed used systems and their complexity. *Probability in the Engineering and Informational Sciences*, **39**(1), 122–140.

27. Pakdaman, Z., and Alizadeh Noughabi, R. (2025c). Analyzing the cumulative residual extropy of system inactivity times and revealing system complexity. *Journal of Inequalities and Applications*, **2025(1)**, 117.

28. Pakdaman, Z., and Hashempour, M. (2021). Mixture representations of the extropy of conditional mixed systems and their information properties. *Iranian Journal of Science and Technology, Transactions A: Science*, **45(3)**, 1057–1064.

29. Qiu, G. (2017). The extropy of order statistics and record values. *Statistics and Probability Letters*, **120**, 52–60.

30. Qiu, G. and Jia, K. (2018a). The residual extropy of order statistics. *Statistics and Probability Letters*, **133**, 15–22.

31. Qiu, G. and Jia, K. (2018b). Extropy estimators with applications in testing uniformity. *Journal of Non-parametric Statistics*, **30**, 182–196.

32. Qiu, G., Wang, L., and Wang, X. (2019). On extropy properties of mixed systems. *Probability in the Engineering and Informational Sciences*, **33**, 471–486.

33. Rao, M., Chen, Y., Vemuri, B. C., and Wang, F. (2004). Cumulative residual entropy: A new measure of information. *IEEE Transactions on Information Theory*, **50**(6), 1220–1228.

34. Rao, T. V. and Naqvi, S. (2024). Preservation of mean inactivity time ordering for coherent systems. *Advances in Applied Probability*, **56**(2), 666–692.

35. Rudin, W. (1964). *Principles of Mathematical Analysis* (2nd ed.). McGraw-Hill.

36. Samaniego, F. J. (1985). On closure of the IFR class under formation of coherent systems. *IEEE Transactions on Reliability*, **34**, 69–72.

37. Samaniego, F. J., Balakrishnan, N. and Navarro, J. (2009). Dynamic signatures and their use in comparing the reliability of new and used systems. *Naval Research Logistics*, **56**, 577–591.

38. Saranya, P., and Sunoj, S. M. (2024). On Relative Cumulative Extropy, Its Residual (Past) Measures and their Applications in Estimation and Testing. *Journal of the Indian Society for Probability and Statistics*, **25**(1), 199–225.

39. Samaniego, F. J. (2007). *System Signatures and Their Applications in Engineering Reliability*. Springer, New York.

40. Shaked, M. and Shanthikumar, J. G. (2007). *Stochastic Orders*. Springer, New York.

41. Shannon, C. (1948). A mathematical theory of communication. *The Bell System Technical Journal*, **27**(3), 379–423.

42. Silverman, B. W. (1986). *Density Estimation for Statistics and Data Analysis*. Chapman & Hall, London.

43. Tavangar, M. (2015). Conditional inactivity time of components in a coherent operating system. *IEEE Transactions on Reliability*, **65**(1), 359–369.

44. Toomaj, A. and Atabay, H. A. (2022). Some new findings on the cumulative residual Tsallis entropy. *Journal of Computational and Applied Mathematics*, **400**, 113669.

45. Toomaj, A. (2023). Generalized cumulative residual Tsallis entropy and its properties. *Computational and Applied Mathematics*, **42**(8), 330.

46. van der Vaart, A. W. (1998). *Asymptotic Statistics.* Cambridge University Press, Cambridge.

47. van der Vaart, A. W., and Wellner, J. A. (1996). *Weak Convergence and Empirical Processes.* Springer, New York.

48. Zhang, Z. (2010). Ordering conditional general coherent systems with exchangeable components. *Journal of Statistical Planning and Inference*, **140**, 454–460.

49. Zhang, Z. and Yang, Y. (2010). Ordered properties of the residual lifetime and inactivity time of k-out-of-n systems under double monitoring. *Statistics and Probability Letters*, **80**, 711–717.

50. Zhang, Z. (2025). The residual life and inactivity time of coherent systems. *Conditional Order Statistics and Conditional Spacings*, Singapore: Springer Nature Singapore, 9–66.

51. Wand, M. P., and Jones, M. C. (1995). *Kernel Smoothing.* Chapman & Hall, London.